

# Direct measurement of sub-pixel structure of the EPIC MOS CCD on-board the XMM/NEWTON satellite

J. HIRAGA <sup>a,1</sup> H.TSUNEMI <sup>a</sup> A.D.SHORT <sup>b</sup> A.F.ABBEY <sup>b</sup>  
P.J.BENNIE <sup>b</sup> M.J.L.TURNER <sup>b</sup>

<sup>a</sup>*Department of Earth and Space Science, Graduate School of Science, Osaka  
University, 1-1 Machikaneyama-cho, Toyonaka, Osaka 5600043, Japan  
CREST, Japan Science and Technology Corporation (JST)*

<sup>b</sup>*Space Reserch Centre, University of Leicester, Leicester, LE1 7RH, UK*

---

## Abstract

We have used a mesh experiment in order to measure the sub-pixel structure of the EPIC MOS CCDs on-board the XMM/NEWTON satellite. The EPIC MOS CCDs have  $40\ \mu\text{m}$ -square pixels which have an open electrode structure in order to improve the detection efficiency for low-energy X-rays. We obtained restored pixel images for various X-ray event grades (e.g. split-pixel events, single pixel events, etc.) at various X-ray energies.

We confirmed that the open electrode structure results in a distorted horizontal pixel boundary. The open electrode region generates both single pixel events and vertically split events, but no horizontally split events. Because the single pixel events usually show the best energy resolution, we discuss a method of increasing the fraction of single pixel events from the open electrode region. Furthermore, we have directly measured the thickness of the electrodes and dead-layers by comparing spectra from the open electrode region with those from the other regions: electrodes, electrode finger and channel stop. We can say that EPIC MOS CCDs are more radiation hard than front-illumination chips of ACIS on-board Chandra X-ray Observatory because of their extra absorption thickness above the charge transfer channel. We calculated the mean pixel response and found that our estimation has a good agreement with that of the ground calibration of EPIC MOS CCD.

*Key words:* charge-coupled device, mesh experiment, open electrode structure  
PACS; 07.85.-m, 29.30.Kv

---

<sup>1</sup> Partially supported by JSPS Research Fellowship for Young Scientists, Japan.

## 1 Introduction

Charge-coupled devices (CCDs) in use in X-ray astronomy combine moderate energy resolution with good spatial resolution[1]. Thanks to these characteristics, they have become a standard X-ray photon counting detector. When an X-ray photon is photoabsorbed inside a CCD, a number of electrons proportional to the incident X-ray energy are liberated. In this way, the energy of an X-ray photon can be measured. Because optical photons can produce only a few electrons, however, CCDs have no energy resolution at optical wavelengths.

The charge cloud produced by an X-ray photon inside the CCD drifts within the depletion region to the bottom of the potential well of the given pixel, resulting in a detected X-ray event. Due to the diffusion process, the charge cloud has a finite size, which can result in the event being detected in more than one pixel. X-ray events may be therefore classified by ‘grade’ according to the number of pixels in which they are detected. When the entire charge cloud is collected within one pixel, for example, it is referred to as a ‘single pixel event’. When the cloud splits into an adjacent horizontal pixel, it is referred to as a ‘horizontally split event’. Similarly, when the cloud splits into an adjacent vertical pixel, it is referred to as a ‘vertically split event’.

A CCD consists of a two dimensional array of small pixels. The spatial resolution is limited by the pixel size which is typically several tens of  $\mu\text{m}$ . The electrode structure, which comprises layers of poly-silicon and silicon-oxide, results in a non-uniformity of detection efficiency over the pixel. In order to measure the structure of one pixel directly, it is therefore necessary to determine the X-ray interaction position on a scale smaller than the pixel size. Recently, we have developed a new technique which allows us to specify the X-ray interaction position with sub-pixel resolution using a two-dimensional mesh containing small holes (much smaller than the CCD pixel size) which are periodically spaced [2]. The sub-pixel structure of various types of CCD (ASCA SIS [3], CHANDRA ACIS [4] and HPK CCD [5]) have been measured using this method.

The X-ray response of a CCD is very sensitive to the thickness of the gate structures within the pixel and is also non-uniform within the pixel. The time-averaged output therefore represents a mean pixel response, rather than the response at any given location within the pixel. Thus the CCD response consists of various parameters which are difficult to measure separately. We have therefore developed the mesh technique in order to measure the response (pixel structure) of CCDs with sub-pixel resolution. This technique has been previously applied to the CCDs [6] employed in the XMM/NEWTON observatory by Tsunemi et al[7]. In this paper, we report on measurements of the sub-

pixel structure of the EPIC MOS CCD with substantially improved spatial resolution.

## 2 The EPIC MOS CCD

The XMM/NEWTON satellite was developed by the European Space Agency (ESA) which comprises a membership of 13 European countries. It was launched into a relatively high-earth orbit in December, 1999. Among its instruments are the 3 EPIC imaging spectrometers, which reside in the focal plane, at the foci of the three mirror modules. All carry silicon CCD detectors. One of the cameras utilizes back-illuminated PN CCDs with  $150\ \mu\text{m}$  square pixels and was developed at the Max Plank Institute [8]. The other two cameras carry MOS CCDs (EEV CCD 22s) which were developed primarily by the X-ray Astronomy Group at Leicester University and Marconi Applied Technologies (formerly EEV) in the United Kingdom [6]. The EPIC MOS CCD is a frame transfer, front-illuminated device.

The EPIC MOS CCD is a three phase device. The electrodes, or gates (poly1, poly2 and poly3) are shown schematically in Figure1. The thickness of depletion region is approximately  $37\ \mu\text{m}$  with nominal clock voltages and substrate bias [6].

The most important feature of the EPIC MOS CCD is its ‘open electrode structure’. In order to improve the detection efficiency at low energies, one of the gates, poly3, has been enlarged by partially removing the front face, leaving two ‘holes’ in each pixel. These holes cover 40 % of the pixel area and are separated by a central electrode ‘finger’ comprising polysilicon, oxide and nitride layers. A P-plus dopant is implanted in the etched areas, which pins the surface potential to the substrate potential.

## 3 Experiment

### 3.1 Experimental Setup

A detailed explanation of our mesh experiments may be found in the literature [2][5]. Figure 2 gives a schematic view of the mesh experiment. The mesh experiment consists of a CCD, a metal mesh and a pseudo parallel X-ray beam. The metal mesh employed has periodically spaced holes which are much smaller than the pixel size. The hole spacing is an integer multiple of the CCD

pixel size. The mesh is placed just above the CCD surface, as close to the CCD as practically possible.

The mesh must have an orientation which is slightly rotated with respect to the CCD so that the shadow of the mesh hole on the CCD gradually shifts its position inside the pixel as shown in Fig. 2. In this way, over the CCD dimensions, the X-rays passing through the mesh holes periodically sample the entire pixel. This produces a moire pattern from which the relative alignment between the mesh and the CCD may be determined [3]. An X-ray event detected by the CCD must have come through one of the mesh holes. Taking into account the hole spacing and the pixel size, we can unequivocally determine the hole location for individual X-ray events. We can therefore calculate the X-ray interaction position within the CCD with sub-pixel resolution. The accuracy is limited by the effective mesh hole size which is slightly bigger than the geometrical shape of the hole due to diffraction.

The experiment was performed in a CCD test facility at Leicester University. The EEV CCD 22 has  $600 \times 600$  pixels with each pixel being  $40 \mu\text{m}$  square. A gold mesh was employed which has a thickness of  $10 \mu\text{m}$  and small holes of  $2 \mu\text{m}$  diameter. The spacing between the holes was  $120 \mu\text{m}$ ; just three times the pixel size. We placed the mesh about  $0.5 \text{ mm}$  above the CCD surface and rotated it by about  $1^\circ.7$  from the CCD. The X-ray generator manufactured by KEVEX Inc. was approximately  $3 \text{ m}$  from the CCD and several fluorescence targets were used, generating characteristic X-rays as well as a Bremsstrahlung spectrum. Figure 3 gives an example the spectrum obtained by the mesh experiment using a Ag target with a voltage of  $5 \text{ kV}$ . There are several characteristic emission lines, O-K ( $0.52 \text{ keV}$ ), Al-K ( $1.5 \text{ keV}$ ), Si-K ( $1.8 \text{ keV}$ ) and Ag-L( $2.9 \text{ keV}$ ), superposed on a continuum extending up to  $5 \text{ keV}$ .

The CCD operating conditions were almost identical to those employed on the XMM/NEWTON satellite. During frame integration we apply  $8 \text{ V}$  (high voltage) to poly3 (in Fig.1) only. The other two gates remained un-biased. The CCD chip was cooled to  $-100^\circ\text{C}$  using liquid nitrogen and was driven using duplicate flight electronics.

Tsunemi et al. (1999) performed the mesh experiments using a similar experimental setup [9]. Their experiment used an existing copper mesh with a thickness of  $10 \mu\text{m}$  and holes of  $4 \mu\text{m}$  diameter. The spacing between the holes was  $48 \mu\text{m}$  which is not a multiple of the pixel size. The effective mesh hole at that time was  $7 \mu\text{m}$  in diameter. For this experiment, we have improved the conditions by fabricating a new mesh which may be positioned much closer to the CCD surface with holes  $2 \mu\text{m}$  in diameter. In the new configuration, the effective mesh hole gives about a factor of 3 improvement in spatial resolution over the previous experiment. Furthermore, the hole spacing is much greater, and is an integer multiple of the pixel size, which makes the determination of

the X-ray interaction location within a given pixel much clearer.

## 4 Data Analysis and Discussion

### 4.1 Image Restoration

The mesh technique allows us to determine the X-ray interaction position within the CCD pixel. Furthermore, it samples the entire pixel which enables us to restore the pixel images for the various X-ray energies as well as the various X-ray event-types. In the data analysis, we pick out the characteristic X-ray energies thanks to their good statistics (as summarized in table 1 in order of attenuation length in  $\text{SiO}_2$ ). We then construct restored images for various X-ray event-types; (a) single pixel events, (b) vertically split events, (c) horizontally split events and (d) all X-ray events, as shown in Figure 4. In this figure, each image represents  $2 \times 2$  pixels of the CCD, with the dashed square corresponding to the pixel size of  $40 \mu\text{m}$  square. Brighter regions correspond to a higher detection efficiency.

Looking at the pixel image restored using all X-ray events (the right hand column), we can clearly see absorption features within the pixel. In particular, the two etched regions in each pixel are clearly visible in the O-K image, since O-K has the shortest attenuation length of the X-ray energies employed. Moving to greater attenuation lengths, the etched region becomes less obvious. It is difficult to see the enhanced region in the Ag-L image which is almost free from absorption within the gate structure.

In the restored image using single pixel events, we clearly see the enhanced region only in the O-K image. Other than the gate structure, we notice that there are three regions in each pixel: the regions generating single pixel events, vertically split events and horizontally split events. Split events are generated in the regions within the pixel where the charge cloud splits into adjacent pixels. We can clearly see that the horizontal pixel boundary (giving rise to vertically split events) is not a straight line but is instead a wavy line. In contrast to this, the vertical pixel boundary is governed by the channel stops, which include a P-plus implant in order to make an electric potential ‘barrier’ which results in a normal (i.e. straight line) shape for the pixel boundary. There are small gaps in the region generating horizontally split events. These correspond to the pixel corners where the 3- or 4-pixel events are generated.

The wavy boundary is due to the fact that the poly3 gate is etched so that it has a finger structure as shown in Fig.1. In other words, the potential generated by poly3 during integration defines a wavy boundary between adjacent pixels

rather than a straight line. The shape of the region generating vertically split events also depends on the attenuation length of the X-rays indicating the depth dependence of the electric field inside the CCD. It can be compared with that expected from the model calculation.

#### *4.2 Spectra from Various Regions inside the Pixel*

In the mesh experiment, we can identify both the energy and the interaction position within the pixel for an individual X-ray photon. We can therefore extract X-ray spectra from any region within the pixel. We selected five regions within the pixel in order to measure the pixel structure of the CCD. These are labeled in Figure 5 as ‘finger’, ‘channel stop’, ‘electrode’, ‘open electrode 1’ and ‘open electrode 2’, respectively. Among them, the channel stop and the finger are so narrow that the selected regions partially overlap with the open electrode region due to the finite spatial resolution of the experiment. Figure 6 shows the spectra for each region using the same data in Fig. 3.

We first compared spectra for the open electrode 1 and 2. We confirmed that the ratio shown in Figure 7 is almost constant and independent of energy. Because these two regions must show the highest efficiency at low energies, we added them together to generate a standard spectrum for the open electrode with which we compare other data. Figure 8 shows the ratio between the spectra for the open electrode and those for other three regions: upper panel, middle panel and lower panel are results of electrodes, finger and channel stop, respectively. Since these figures represent the extra absorption features in each region, we fitted them with a relatively simple absorption model. The model contains a normalization, a constant component and absorption features for Si and SiO<sub>2</sub>. The normalization is required due to the difference in area of each region and the constant comes from the area of overlap with the open electrode region. In this way, we obtained the thickness of Si and SiO<sub>2</sub> for each region. The best fit results are shown in Fig. 8 by solid lines and summarized in Table 2.

#### *4.3 Radiation Hardness*

In June 1999 the Chandra X-ray Observatory (CXO) was launched into a high-earth orbit, similar to that of the XMM/NEWTON satellite. It is equipped with a CCD camera (ACIS) consisting of ten CCD chips: eight front-illuminated (FI) CCDs and two back-illuminated (BI) CCDs. In august, it was reported that a substantial degradation of the CCD had occurred [11]. The degree of the degradation is worse than that for the ASCA CCDs, despite that ASCA has been in a low-earth orbit since February, 1993. It should be

noted that the FI CCDs are heavily damaged while the BI CCDs are free from damage. It was concluded that the degradation was due to a relatively high flux of low energy ( $\sim 100$  keV) protons. The interpretation is that the low energy protons are collected onto the CCD and penetrate the relatively thin electrode structure leaving traps near the charge transfer channel.

The charge transfer channel is a relatively narrow path inside the pixel that is localized as a ‘notch’ structure [12]. The effective thickness of the electrode structure above the charge transfer channel is directly measured by the mesh experiment and found to be  $\sim 0.3 \mu\text{m}$  thick Si and  $\sim 0.3 \mu\text{m}$  thick  $\text{SiO}_2$  [4]. Therefore, the high flux of low energy protons penetrates this structure and causes permanent damage on the buried channel of the CCD. In the case of the BI CCD, the charge transfer channel is relatively far away from the entrance side, resulting in no damage to these CCDs.

The EPIC MOS CCD has a complicated electrode structure. The effective thickness of the absorber above the open electrode structure is designed to be  $\sim 0.085 \mu\text{m}$  thick  $\text{SiO}_2$ . This indicates that low energy protons will easily generate traps under the open electrode structure. However, the charge transfer channel is just under the finger structure. Our measurements indicate that the finger structure consists of  $\sim 0.2 \mu\text{m}$  thick Si and  $\sim 0.7 \mu\text{m}$  thick  $\text{SiO}_2$ . This indicates that the charge transfer channel of the EPIC MOS CCD is better protected than that of the ACIS CCD. We can say that the EPIC-MOS CCD is more radiation hard than the FI chip of the ACIS. The details on the radiation hardness requires more quantitative measurement.

#### 4.4 Application

X-ray events detected by a CCD are classified by the number of pixels over which the resultant charge splits. Due to readout noise and charge loss around the charge cloud perimeter, single pixel events generally give the best energy resolution. One of the main features of this CCD is its open electrode region where the low energy efficiency is enhanced. We must therefore endeavour to control the operating conditions so that we can increase the active region generating single pixel events in the open electrode.

Fig. 4 clearly shows that vertically split events are generated primarily in the open electrode. Furthermore, the shape of this region depends on the attenuation length of the photon in Si. This must be due to the interaction of the applied voltages on neighbouring electrodes. In the standard mode, poly3 is biased during integration while the other two electrodes are not. We performed an experiment in which we biased both poly3 and poly1 during integration. Figure 9 shows the restored images for Mo-L(2.3keV) X-ray events

again classified by X-ray event-type as in Fig. 4. It is clear that the horizontal pixel boundary for vertically split events has been changed. We have not yet been able to determine which working condition is the best for spectroscopic study. This will require further study, taking into account the effect of the thickness of the depletion region.

In the mesh experiment, we can study how the primary charge behaves inside the CCD [10]. In some pixel regions, when the primary charge is photoabsorbed close to the front surface of the device, it produces a tail in the spectrum. This effect is more evident for low energy X-rays since they have a shorter attenuation length in Si. In particular, the response of the O-K line shows a strong dependence on the interaction position within the pixel. In our experiment, the incident X-ray spectrum contains several emission lines as well as a relatively strong continuum which prevents us from studying in detail any tail to the response function. In order to study this, we require a mono-energetic X-ray beam. The present experimental setup does not currently permit us to generate such mono-energetic X-ray beams with sufficient flux to conduct the mesh experiment.

#### 4.5 *Detection Efficiency*

We calculated the mean pixel response that is shown in Figure 10 with taking into account our results of each structure within the pixel; open-electrodes, electrodes, finger and channel stop. It was calculated with parameters measured from the mesh experiment as described in table 2 weighted with area fractions of each structure. In this calculation, we assumed that there is an extra absorption of  $\sim 0.085 \mu\text{m}$  thick  $\text{SiO}_2$  and  $\text{Si}_3\text{N}_4$  over the pixel since we can not measure the absorption on the open electrode region. These extra absorption play an important role of the absorption feature at the low energy region. We also assume that the depletion region is  $37 \mu\text{m}$  [6] thick that plays an important role at the high energy region.

We compared our result with that reported by C. Pignatelli et al. 1999 [13] which performed the ground calibrations of EPIC MOS CCD using mono-energetic X-ray beam at Osay synchrotron facility in France. We found that our estimation has a good agreement with the data points of their ground calibration.

## 5 Conclusion

We performed a mesh experiment on a CCD CCD identical to that employed in the EPIC MOS imaging spectrometers on-board XMM/NEWTON. We

were able to obtain restored X-ray images with sub-pixel resolution using X-ray photons of characteristic emission lines: O-K, Y-L, Mo-L, Al-K and Ag-L. All the X-ray events are classified by their event-types: single pixel event, horizontally split event, vertically split event and all events. There are clear absorption features inside the pixel including electrodes, channel stops etc. The shorter the attenuation length in SiO<sub>2</sub>, the clearer these absorption features become.

We also confirmed that the horizontal pixel boundary between vertically split events is not a straight line, but is ‘wavy’. The specific shape of this wavy line depends on the attenuation length of the X-ray photons in silicon. This indicates the depth dependence of the electric field inside the CCD. We obtained spectra from various regions within a CCD pixel, which showed a non-uniformity of the detection efficiency. We selected five regions from which we extracted spectra. We then compared the spectrum from the open electrode region with the other regions in order to measure the absorption features in detail. The electrode structure comprises  $0.29 \pm 0.03 \mu\text{m}$  of Si and  $0.94 \pm 0.05 \mu\text{m}$  of SiO<sub>2</sub> while the electrode finger comprises  $0.15 \pm 0.05 \mu\text{m}$  of Si and  $0.73 \pm 0.02 \mu\text{m}$  of SiO<sub>2</sub>. The effective absorption at the channel stop is equivalent to  $0.57 \pm 0.03 \mu\text{m}$  of SiO<sub>2</sub>.

The charge transfer channel is a relatively narrow path within the pixel; just below the electrode finger in the case of EPIC MOS CCD. We found that the extra absorption feature above the charge transfer channel of EPIC MOS CCD is thicker than that of the FI CCD of ACIS ( $\sim 0.3 \mu\text{m}$  of Si and SiO<sub>2</sub>) on-board the CXO whose orbit is similar to that of XMM/NEWTON. For the ACIS CCD, it was reported that FI CCDs got permanent damages on the buried channel due to a relatively high flux of low energy protons. Our measurement indicates that the EPIC MOS CCD is more radiation hard than the FI CCD of the ACIS.

In the standard working condition of the CCD, the vertically split events are generated mainly in the open electrode region where the detection efficiency at low energies is enhanced. Since single pixel events usually give better energy resolution than split pixel events, it is preferable to generate more single events and less split events in the open electrode region. We confirmed that the shape of the region generating the vertically split event varies by changing the operation mode. We can therefore control the CCD so that the open electrode region generates more single pixel events rather than split events.

We calculated the mean pixel response based on our measurement. Our estimation has a good agreement with that performed on the ground calibration of the EPIC MOS CCD using mono-energetic X-ray beam.

## Acknowledgements

This research was partially supported by Simitomo Foundation.

## References

- [1] G. W. Frazer: X-ray Detectors in Astronomy (Cambridge University Press, Cambridge, 1989) p. 208.
- [2] H. Tsunemi, K. Yoshita, S. Kitamoto, *Jpn. J. Appl. Phys.* **36** (1997) 2906.
- [3] K. Yoshita, H. Tsunemi, K. C. Gendreau, G. Pennington and M. W. Bautz, *IEEE Trans. Nucl. Sci.*, **45**, (1998) 915.
- [4] M. J. Pivovarov, S. Jones, M. Bautz, S. Kissel, G. Prigozhin, G. Ricker, H. Tsunemi and E. Miyata, *IEEE Trans. Nucl. Sci.*, **45**, (1998) 164.
- [5] H. Tsunemi, K. Yoshita, J. Hiraga, S.Kitamoto, *Jpn. J. Appl. Phys.* **37** (1998) 2734.
- [6] A. D. Short, A. Keay, M. J. L. Turner, *Proc. SPIE*, **3445**, (1998) 13.
- [7] K. O. Mason, G. Bignami, A. C. Brinkman, A. Peacock, *Advances in Space Research*, **16**, (1995) 41.
- [8] E. Pfeffermann et al.,*Proc. SPIE*, **3765**, (1999) 184.
- [9] H. Tsunemi, K. Yoshita, A.D. Short, P.J. Bennie, M.J.L Turner and A.F. Abbey, *Nucl. Instr. and Meth. A*, 437 (1999) 359-366.
- [10] M.Bautz et al.,*Nucl. Instr. and Meth. A*, 436 (1999) 40-52
- [11] S.L.O'Dell et al.,*Proc. SPIE*, **4140**, (2000) in press.
- [12] B. E. Burke et al. *IEEE Trans. Electron Devices*, **44**,(1997) 1633.
- [13] C.Pigiot et al.,*Proc. SPIE*, **3765**, (1999)

Table 1  
 Summary of characteristic X-ray energies obtained.

Characteristic X-ray	Energy [keV]	Attenuation	
		length in Si [ $\mu\text{m}$ ]	length in SiO <sub>2</sub> [ $\mu\text{m}$ ]
O-K	0.52	0.47	0.93
Y-L	1.9	1.4	2.4
Mo-L	2.3	2.2	3.9
Al-K	1.5	7.9	4.2
Ag-L	2.9	4.4	7.9

Table 2

The extra thickness of various regions within the pixel

Selected region	thickness of Si [ $\mu\text{m}$ ]	thickness in SiO <sub>2</sub> [ $\mu\text{m}$ ]
Electrodes	$0.29 \pm 0.03$	$0.94 \pm 0.05$
Finger	$0.15 \pm 0.05$	$0.73 \pm 0.02$
Channel stop	–	$0.57 \pm 0.03$

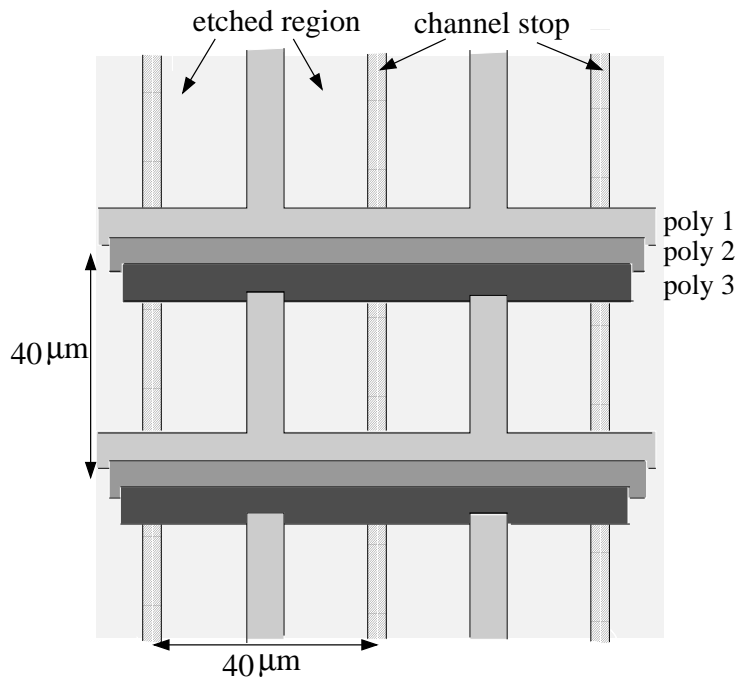


Fig. 1. Schematic structure inside the pixel of an EPIC MOS CCD. There are three electrodes: one is partly etched in order to improve detection efficiency at low energy.

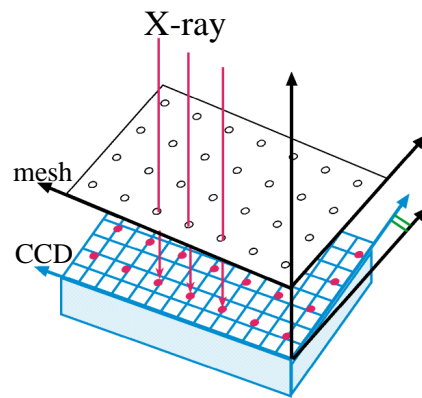


Fig. 2. Schematic view of the mesh experiment showing the orientation of the mesh with respect to the CCD. The X-ray landing position is restricted by the mesh hole.

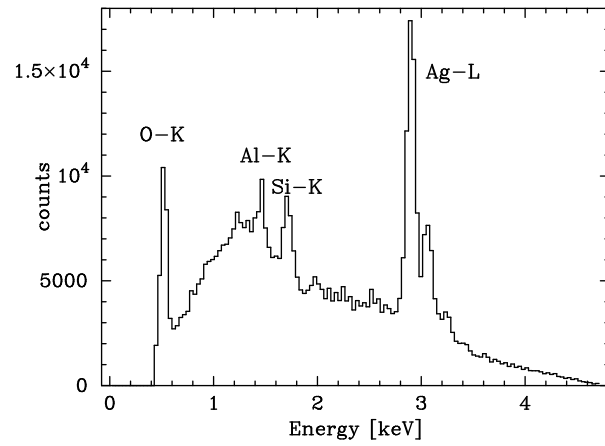


Fig. 3. Energy spectrum obtained using the whole CCD data. There are several characteristic emission lines, O-K (0.52 keV), Al-K (1.5 keV), Si-K (1.8 keV) and Ag-L(2.9 keV), superposed on a continuum extending up to 5 keV.

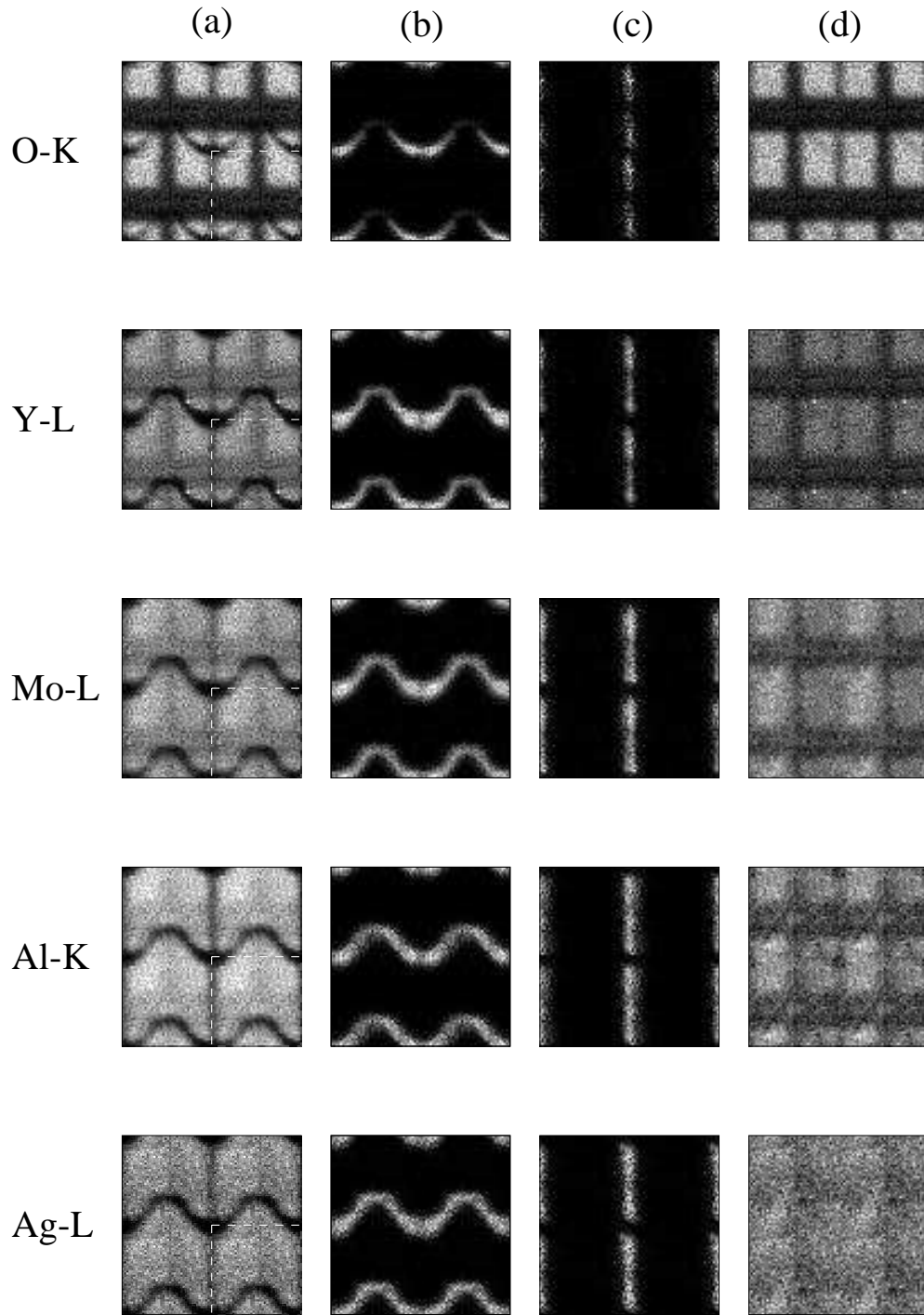


Fig. 4. Restored images using characteristic X-ray emission lines for various X-ray event-types; (a) single pixel events, (b) vertically split events, (c) horizontally split events and (d) all X-ray events. The results are sorted by the order of the attenuation length in  $\text{SiO}_2$ . Each image represents  $2 \times 2$  pixels of the CCD, with the dashed square corresponding to the pixel size of  $40 \mu\text{m}$  square.

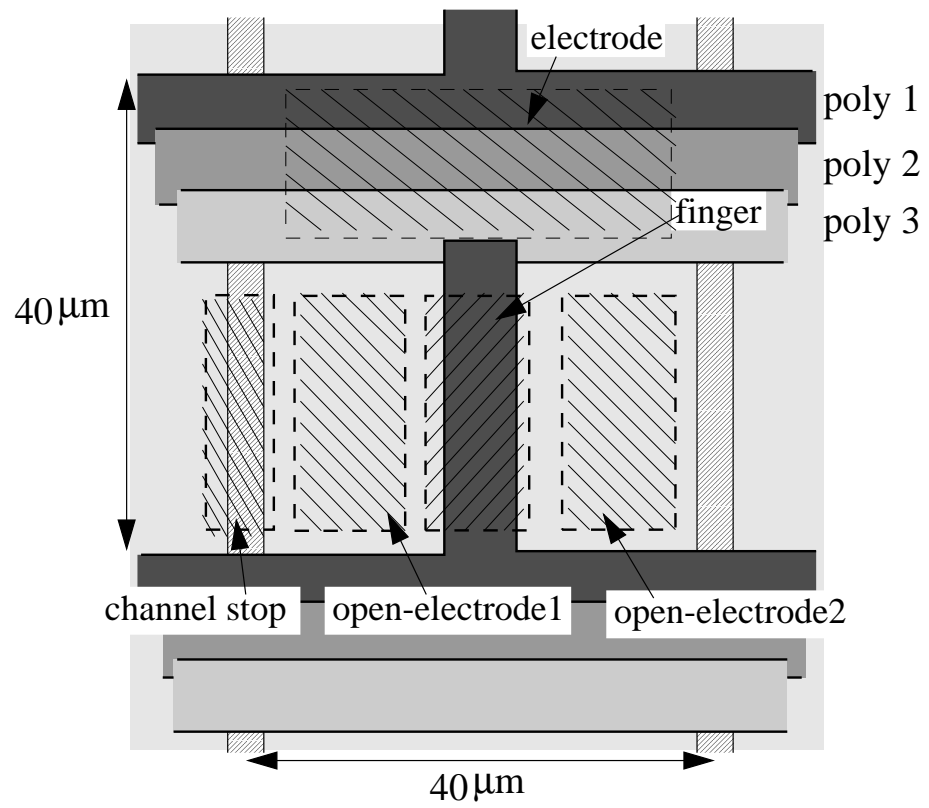


Fig. 5. Five selected regions within the pixel are shown. They are taking into account the electrodes or channel stop structure to compare spectra to each other.

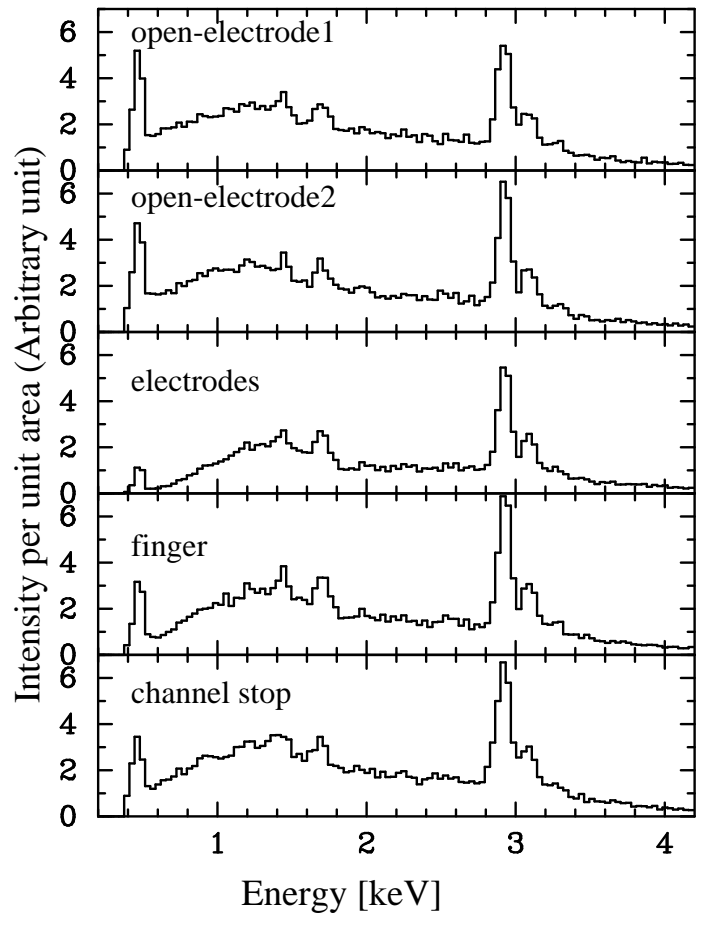


Fig. 6. Spectra from five selected regions within the pixel.

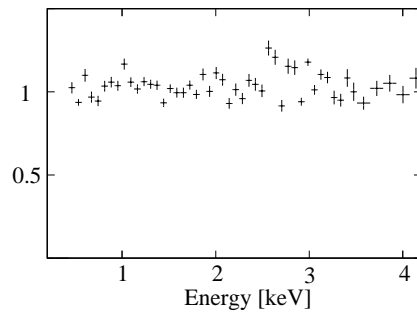


Fig. 7. Ratio between the spectrum obtained at the open electrode 1 and that obtained at the open electrode 2.

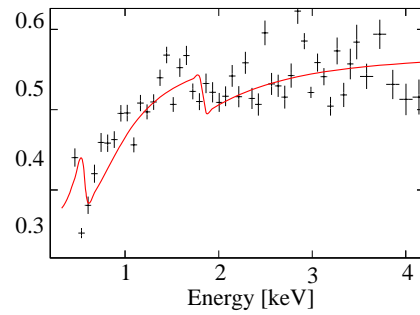
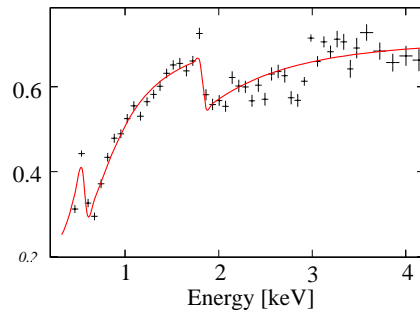
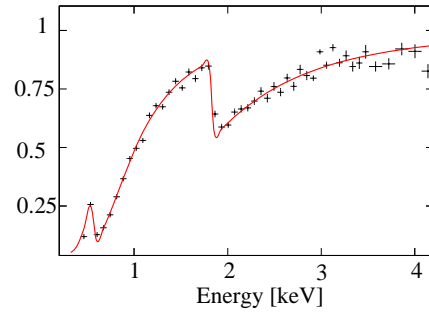


Fig. 8. Ratios between the spectrum of the open electrodes and those of selected regions: upper, middle and lower panels represent results of electrodes, finger and channel stop, respectively. Solid lines represent the best fit absorption model.

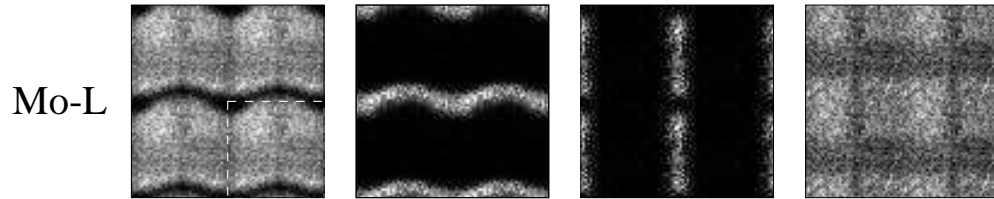


Fig. 9. Same as for Fig.4 for Mo-L (2.3 keV) using the data with another cloaking pattern during integration time.

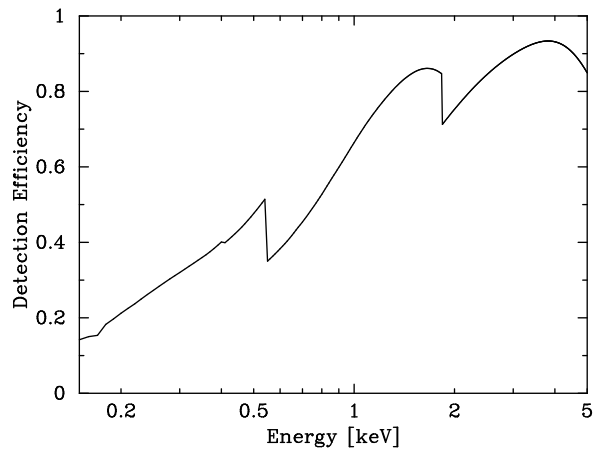


Fig. 10. Mean pixel response calculated based on our results.